

DETRs with Hybrid Matching

Ding Jia^{1†} Yuhui Yuan^{4 †‡} Haodi He^{2†} Xiaopei Wu³ Haojun Yu¹ Weihong Lin⁴
Lei Sun⁴ Chao Zhang¹ Han Hu⁴

¹Peking University ²University of Science and Technology of China ³Zhejiang University
⁴Microsoft Research Asia

Abstract

One-to-one set matching is a key design for DETR to establish its end-to-end capability, so that object detection does not require a hand-crafted NMS (non-maximum suppression) method to remove duplicate detections. This end-to-end signature is important for the versatility of DETR, and it has been generalized to a wide range of visual problems, including instance/semantic segmentation, human pose estimation, and point cloud/multi-view-images based detection, etc. However, we note that because there are too few queries assigned as positive samples, the one-to-one set matching significantly reduces the training efficiency of positive samples. This paper proposes a simple yet effective method based on a hybrid matching scheme that combines the original one-to-one matching branch with auxiliary queries that use one-to-many matching loss during training. This hybrid strategy has been shown to significantly improve training efficiency and improve accuracy. In inference, only the original one-to-one match branch is used, thus maintaining the end-to-end merit and the same inference efficiency of DETR. The method is named H-DETR, and it shows that a wide range of representative DETR methods can be consistently improved across a wide range of visual tasks, including Deformable-DETR, 3DETR/PETRv2, PETR, and TransTrack, among others. Code will be available at: <https://github.com/HDETR>

1. Introduction

Since the success of pioneering work DEtection TRansformer (DETR) [5] on object detection tasks, DETR-based approaches have achieved significant progress on various fundamental vision recognition tasks such as object detection [74, 81, 44, 52], instance segmentation [23, 12, 11, 70], panoptic segmentation [8, 29, 58, 69, 71], referring expression segmentation [63, 67], video instance segmenta-

tion [7, 64, 59], pose estimation [54, 24, 53], multi-object tracking [6, 43, 55], monocular depth estimation [27, 17], text detection & layout analysis [49, 50, 40, 77], line segment detection [65], 3D object detection based on point clouds or multi-view images [46, 1, 61, 28], visual question answering [21, 41], and so on.

Motivated by the success of DETR on a wide variety of vision tasks, many follow-up efforts have improved DETR from various aspects, including redesigning more advanced transformer encoder [81, 13, 14] or transformer decoder architectures [44, 73, 81, 4] or query formulations [62, 34, 22, 74]. Different from most of these previous efforts, we focus on the inefficient training issues caused by one-to-one matching, which only assigns one query to each ground truth. For example, Deformable-DETR typically only selects less than 30 queries from a pool of 300 queries to match with the ground truth for each image, as nearly 99% of the COCO images consist of less than 30 bounding boxes annotations, while the remaining more than 270 queries will be assigned as \emptyset and are supervised with only classification loss, thus suffering from very limited localization supervision.

To overcome the drawbacks of one-to-one matching and unleash the benefits of exploring more positive queries, we present a very simple hybrid matching scheme to produce more informative queries that are matched with ground truth within each forward pass. The key insight of hybrid matching is to use one-to-many matching to increase the training efficiency and use one-to-one matching to avoid NMS. We mainly propose a very simple yet surprisingly effective hybrid-branch scheme to unify a one-to-one matching manner and a one-to-many matching manner with two different decoder branches. During the training phase, we maintain one decoder branch to process a group of queries for one-to-one matching and another decoder branch to process an additional group of queries for one-to-many matching. During the evaluation, we only use the first decoder branch accompanied by the first group of queries that are supervised with the one-to-one matching scheme, thus not only avoiding NMS but also bringing zero additional computa-

[†]Equal contribution.

[‡] {yuhui.yuan, hanhu}@microsoft.com

Table 1: Illustrating the improvements of our hybrid matching scheme across four challenging vision tasks. All the improvements are obtained under the same training epochs and do not require any additional computation cost during evaluation.

Tasks	2D object detection		2D pose estimation		3D object detection		multi-object tracking	
Methods	Deformable-DETR [81]		PETR [53]		PETRv2 [37]		3DETR-m [46]	TransTrack [55]
Datasets (metrics)	COCO (AP)	LVIS (AP)	COCO (AP)		nuScenes (NDS)	ScanNetV2 (AP ₅₀)	MOT17 (MOTA)	
Baseline	47.0	43.7	73.3		50.68	45.45	67.1	
Ours	48.7	47.5	74.9		52.38	47.01	68.7	
△	+1.7	+3.8 ^b	+1.6		+1.7	+1.56	+1.6	

^b: Part of the gains is obtained with other tricks and we provide more details in the experiments and supplementary.

tion overhead during inference. Besides, we further introduce another two simple variants of the hybrid matching scheme, including the hybrid-epoch scheme and the hybrid-layer scheme.

Last, to demonstrate the effectiveness of our approach, we apply our hybrid matching scheme to various DETR-based approaches, including Deformable-DETR [81] designed for image object detection, 3DETR [46] designed for 3D object detection from point clouds, PETRv2 [37] designed for 3D object detection from multi-view images, PETR [53] designed for multi-person pose estimation, and TransTrack [55] designed for multi-object tracking. Our approach consistently achieves significant gains over most of them and we briefly summarize some representative results in Table 1. For example, our approach improves the very recent multi-view images based 3D detection framework PETRv2 from 50.68% to 52.38% on nuScenes val.

2. Related work

DETR for object detection. With the pioneering work DETR [5] introducing transformers [57] to 2D object detection, more and more follow-up works [44, 13, 10, 62] have built various advanced extensions based on DETR because it removes the need for many hand-designed components like non-maximum suppression [47] or initial anchor boxes generation [16, 51, 32, 35]. Deformable-DETR [81] introduced the multi-scale deformable self/cross-attention scheme, which attends to only a small set of key sampling points around a reference and achieves better performance than DETR (especially on small objects). DAB-DETR [34] further verified that a different novel query formulation can also improve the performance. The follow-up DINO-DETR [22, 74] has established the new SOTA results on object detection tasks and demonstrated the advantages of DETR design by introducing a novel query denoising scheme. Different from these works, we focus on the matching mechanism design of DETR and propose a very simple strategy to improve the training efficiency while still avoiding NMS, which also differentiates our efforts from the very recent DE-DETR [60] that requires NMS.

DETR for 3D object detection based on point-cloud or multi-view-images. The basic goal of 3D object detection is to identify and localize objects in 3D scenes that can be represented using point clouds or multi-view images. How to apply DETR for 3D object detection has attracted a lot of efforts [46, 20, 19, 1, 38, 31, 36]. 3DETR [46] introduced two important changes to the standard DETR [5], including non-parametric query embeddings and Fourier positional embeddings. The concurrent GroupFree3D [39] also showed the advantages, i.e., point grouping-free, of transformer for 3D object detection from the irregular point cloud. DETR3D [61] successfully introduced the DETR to address the 3D object detection based on multi-view images, which exploits camera transformation matrices of multi-view images and links them to 3D positions. The follow-up BEVFormer [28] further extended DETR3D via exploiting spatial and temporal information and interacting with spatial and temporal space with a set of predefined grid-shaped BEV queries. We choose two representative open-sourced SOTA methods, including 3DETR [46] and PETRv2 [36, 37], to verify the generalization ability of our approach on 3D object detection.

DETR for pose estimation. The objective of the pose estimation task is to localize the key points of the presented persons in a given image. Multi-person pose estimation requires further grouping of the key points of the same person. Many recent efforts [54, 2, 24, 75, 26] have verified the potential of DETR for pose estimation. For example, POET [54] extended DETR from object detection to multi-person pose estimation by introducing a novel loss function and a pose representation. TFPose [42] showed that Deformable-DETR is a strong baseline for single-person pose estimation task. PETR [53] proposed to treat the pose estimation task as a hierarchical set prediction problem and designed a set of pose queries for decoding the full-body poses and a joint query for refining the predictions via exploring the structured relations between different key points. We also choose PETR [53] to verify the generalization ability of our approach to pose estimation task as PETR is a representative fully end-to-end multi-person pose estimation framework and sets strong results in terms of a

speed-accuracy trade-off.

DETR for object tracking. Object tracking aims at locating the objects across both spatial and temporal positions within a given video without any prior knowledge about the appearance and number of targets. STARK [66, 78] built a spatial-temporal tracking scheme, based on DETR, to exploit spatial and temporal information simultaneously to address the single object tracking problem. TransTrack [55] and TrackFormer [43] proposed to use a set of track queries to associate the detected objects along temporal dimensions except using the original object queries to locate the objects within each frame respectively. MOTR [72] also extended DETR and introduced track queries to model the tracked objects in the entire video. To verify the generalization ability of our approach to object tracking task, we apply our approach to the representative TransTrack [55] approach.

Label assignment. We can categorize the existing label assignment approaches, following the previous work [59, 80], into two different paths: (i) *one-to-many label assignment*, i.e., assigning multiple predictions as positive samples for each ground-truth box. We can further divide most one-to-many label assignment strategies into two sub-paths including fixed label assignment, e.g., Faster R-CNN [51] assigns the anchors as positive/negative samples by comparing their IoUs to a pre-defined threshold such as 0.5. FCOS [56] simply treats the anchors close to the object centers as positive samples; and dynamic label assignment, e.g., ATSS [76] exploits the statistical characteristics of an object to divide the anchors into positive and negative samples automatically without any hyper-parameter. (ii) *one-to-one label assignment*, i.e., assigning only one prediction as a positive sample for each ground-truth box. POTO [59] propose to assign the anchor with either the maximum IoU or closest to the object center as the positive sample, which is modified from the strategies of RetinaNet [32] or FCOS. DETR [5] and its followups [44, 4, 62, 81, 34, 22] apply the Hungarian matching to compute one-to-one positive assignments based on the global minimum matching cost values between all predictions and the ground-truth boxes. Different from the most related work POTO [59] that only uses one-to-many assignment, based on ATSS [76], to help the classification branch of FCOS [56], our approach chooses Hungarian matching to perform both one-to-one matching and one-to-many matching following DETR and generalizes to various vision tasks.

3. Our Approach

3.1. Preliminary

General DETR pipeline. Given an input image \mathbf{I} , DETR first applies the backbone and the transformer encoder to

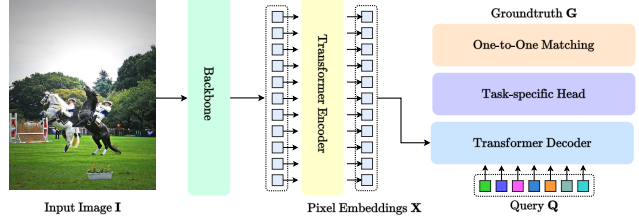


Figure 1: Illustrating the pipeline of DETR.

extract a sequence of enhanced pixel embeddings $\mathbf{X} = \{\mathbf{x}_0, \mathbf{x}_1, \dots, \mathbf{x}_N\}$. Second, DETR sends the enhanced pixel embeddings and a default group of object query embeddings $\mathbf{Q} = \{\mathbf{q}_0, \mathbf{q}_1, \dots, \mathbf{q}_n\}$ into the transformer decoder. Third, DETR applies the task-specific prediction heads on the updated object query embeddings after each transformer decoder layer to generate a set of predictions $\mathbf{P} = \{\mathbf{p}_0, \mathbf{p}_1, \dots, \mathbf{p}_n\}$ independently. Last, DETR performs one-to-one bipartite matching between the predictions and the ground-truth bounding boxes and labels $\mathbf{G} = \{g_0, g_1, \dots, g_m\}$. Specifically, DETR associates each ground-truth with the prediction that has the minimal matching cost and apply the corresponding supervision accordingly. Figure 1 also illustrates the overall pipeline of the DETR approach.

The follow-up works have reformulated the object query to various variants for different vision recognition tasks such as mask query [8, 29], pose query [53], track query [55, 43], bins query [30], and so on. We use “query” in the following discussions for simplicity and consistency.

General Deformable-DETR pipeline. The Deformable-DETR improves the pipeline of DETR from the following three main aspects: (i) replace the original multi-head self-attention or cross-attention with a multi-scale deformable self-attention and multi-scale deformable cross-attention scheme; (ii) replace the original independent layer-wise prediction scheme with iterative refinement prediction scheme; (iii) replace the original image content irrelevantly query with a dynamic query generated by the output from the transformer encoder. Besides, Deformable-DETR also performs one-to-one bipartite matching following the DETR. Readers could refer to [81] for more details.

3.2. Hybrid Matching

The key idea of our hybrid matching approach is to combine the advantages of one-to-one matching scheme with those of one-to-many matching scheme, where the one-to-one matching is necessary for removing NMS and the one-to-many matching enriches the number of queries that are matched with ground truth for higher training efficiency. We first illustrate detailed implementations of the hybrid

branch scheme, and then briefly introduce the implementations of another two simple variants, including the hybrid epoch scheme and hybrid layer scheme. We summarize the pipelines of these hybrid matching schemes in Figure 2.

3.2.1 Hybrid Branch Scheme

We maintain two groups of queries $\mathbf{Q}=\{\mathbf{q}_1, \mathbf{q}_2, \dots, \mathbf{q}_n\}$ and $\widehat{\mathbf{Q}}=\{\widehat{\mathbf{q}}_1, \widehat{\mathbf{q}}_2, \dots, \widehat{\mathbf{q}}_T\}$, where we apply one-to-one matching or one-to-many matching on the predictions based on \mathbf{Q} or $\widehat{\mathbf{Q}}$ respectively.

One-to-one matching branch. We process the first group of queries \mathbf{Q} with L transformer decoder layers and perform predictions on the output of each decoder layer respectively. Then, we perform the bipartite matching between the {predictions, ground-truth} pair over each layer, e.g., estimating $\mathcal{L}_{\text{match}}(\mathbf{P}^l, \mathbf{G})$, and compute the loss as follows:

$$\mathcal{L}_{\text{one2one}} = \sum_{l=1}^L \mathcal{L}_{\text{Hungarian}}(\mathbf{P}^l, \mathbf{G}), \quad (1)$$

where \mathbf{P}^l represents the predictions outputted by the l -th transformer decoder layer. We choose $\mathcal{L}_{\text{match}}(\cdot)$ and $\mathcal{L}_{\text{Hungarian}}(\cdot)$ following DETR [5] and Deformable-DETR [81], which consist of a classification loss, a \mathcal{L}_1 regression loss, and a GIoU loss.

One-to-many matching branch. Then, we process the second group of queries $\widehat{\mathbf{Q}}$ with the same L transformer decoder layers and get L groups of predictions. In order to perform one-to-many matching, we simply repeat the ground truth for K times and get an augmented target $\widehat{\mathbf{G}}=\{\mathbf{G}^1, \mathbf{G}^2, \dots, \mathbf{G}^K\}$, where $\mathbf{G}^1=\mathbf{G}^2=\dots=\mathbf{G}^K=\mathbf{G}$. We also perform the bipartite matching between the {predictions, augmented ground truth} pair over each layer, e.g., estimating $\mathcal{L}_{\text{match}}(\widehat{\mathbf{P}}^l, \widehat{\mathbf{G}})$, and compute the corresponding loss as follows:

$$\mathcal{L}_{\text{one2many}} = \sum_{l=1}^L \mathcal{L}_{\text{Hungarian}}(\widehat{\mathbf{P}}^l, \widehat{\mathbf{G}}), \quad (2)$$

where $\widehat{\mathbf{P}}^l$ represents the predictions output by the l -th transformer decoder layer.

In summary, we use the combination of the above two losses, i.e., $\lambda \mathcal{L}_{\text{one2many}} + \mathcal{L}_{\text{one2one}}$, through the whole training process. To accelerate the training speed and process both \mathbf{Q} or $\widehat{\mathbf{Q}}$ in parallel, we further apply a masked multi-head self-attention to avoid their interactions. Therefore, we do not observe significant extra training costs in experiments, e.g., the hybrid matching scheme takes ~ 85 minutes for each training epoch while the default one-to-one matching scheme takes ~ 65 minutes. Last, we only keep the one-to-one matching branch, i.e., $\widehat{\mathbf{Q}}$, during evaluation. We present the overall pipeline on the left of Figure 2.

3.2.2 More Variants of Hybrid Matching

Hybrid epoch scheme. Different from the hybrid branch scheme, we only maintain a single group of queries $\widetilde{\mathbf{Q}}=\{\widetilde{\mathbf{q}}_1, \widetilde{\mathbf{q}}_2, \dots, \widetilde{\mathbf{q}}_M\}$, where we apply both one-to-one matching and one-to-many matching on the predictions based on $\widetilde{\mathbf{Q}}$ during different training epochs. We illustrate more details as follows.

- *One-to-many matching training epochs:* During the first ρ training epochs, we perform one-to-many matching to process $\widetilde{\mathbf{Q}}$ with L transformer decoder layers and get L groups of predictions. We also get the augmented ground truth $\widetilde{\mathbf{G}}=\{\mathbf{G}^1, \mathbf{G}^2, \dots, \mathbf{G}^{\widetilde{K}}\}$ following the similar manner adopted by the one-to-many matching branch. Then we perform the bipartite matching between $\mathcal{L}_{\text{match}}(\widetilde{\mathbf{P}}^l, \widetilde{\mathbf{G}})$ and compute the loss as follows:

$$\mathcal{L}_{\text{one2many}} = \sum_{l=1}^L \mathcal{L}_{\text{Hungarian}}(\widetilde{\mathbf{P}}^l, \widetilde{\mathbf{G}}). \quad (3)$$

- *One-to-one matching training epochs:* We change one-to-many matching to one-to-one matching for the remaining $(1-\rho)$ training epochs. The only difference is that we match the predictions with the original ground truth and illustrate the formulation as follows:

$$\mathcal{L}_{\text{one2one}} = \sum_{l=1}^L \mathcal{L}_{\text{Hungarian}}(\widetilde{\mathbf{P}}^l, \mathbf{G}). \quad (4)$$

Last, we directly apply $\widetilde{\mathbf{Q}}$ during evaluations without using NMS. In summary, we apply only $\mathcal{L}_{\text{one2many}}$ or $\mathcal{L}_{\text{one2one}}$ in the first ρ training epochs or last $(1-\rho)$ training epochs respectively. We also illustrate the overall pipeline of the hybrid epoch scheme in the middle of Figure 2.

Hybrid layer scheme. Similar to the hybrid epoch scheme, we also maintain a single group of queries $\widetilde{\mathbf{Q}}=\{\widetilde{\mathbf{q}}_1, \widetilde{\mathbf{q}}_2, \dots, \widetilde{\mathbf{q}}_N\}$. Instead of performing different matching strategies across different training epochs, we apply one-to-many matching on the prediction output by the first L_1 transformer decoder layers and one-to-one matching on the prediction output by the remaining L_2 transformer decoder layers.

- *One-to-many matching decoder layers:* We choose to apply a one-to-many matching scheme for the first L_1 transformer decoder layers, where we supervise the predictions, output by each one of the first L_1 layers, with the augmented ground truth $\overline{\mathbf{G}}=\{\mathbf{G}^1, \mathbf{G}^2, \dots, \mathbf{G}^{\widetilde{K}}\}$ following:

$$\mathcal{L}_{\text{one2many}} = \sum_{l=1}^L \mathcal{L}_{\text{Hungarian}}(\overline{\mathbf{P}}^l, \overline{\mathbf{G}}), \quad (5)$$

where we also need to perform the bipartite matching between $\mathcal{L}_{\text{match}}(\overline{\mathbf{P}}^l, \overline{\mathbf{G}})$ before computing the above loss.

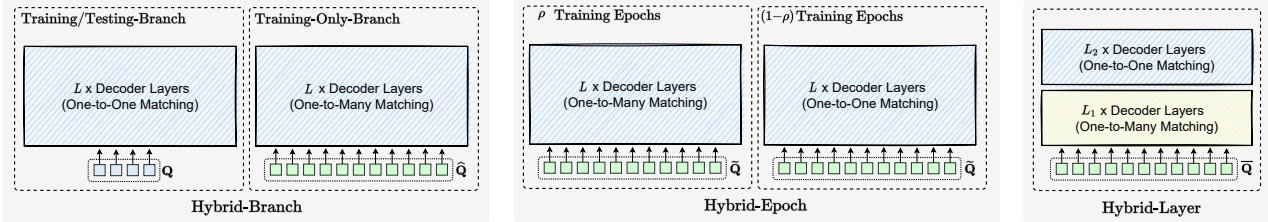


Figure 2: **Illustrating the pipeline of our Hybrid Matching scheme.** We use the colored sketch regions of the same color to mark their parameters are shared. We use ρ to represent the percentage of training epochs. We have $L=L_1+L_2$ in hybrid layer scheme.

Table 2: Improvements comparison based on the proposed hybrid matching approaches. We ensure that three different hybrid approaches all (i) introduce $6\times$ more positive samples than the baseline, and (ii) use 1800 query in total. The upper script \dagger marks the methods using 1800 query during both training and evaluation. The time is averaged over all training epochs as hybrid epoch scheme consists of different training stages. The FPS is tested on the same V100 GPU.

Method	FLOPs	Time (average)	FPS	#epochs		
				12	24	36
Deformable-DETR	268G	65min	6.7	43.7	46.4	46.8
Deformable-DETR \dagger	282G	75min	6.3	44.1	46.6	47.1
Deformable-DETR + Hybrid-Branch	268G	85min	6.7	45.9	47.6	48.0
Deformable-DETR + Hybrid-Epoch \dagger	282G	95min	6.3	45.5	47.0	47.9
Deformable-DETR + Hybrid-Layer \dagger	282G	100min	6.3	45.6	47.9	48.0

- *One-to-one matching decoder layers*: For the following L_2 transformer decoder layers, we perform a one-to-one matching scheme on their predictions as follows:

$$\mathcal{L}_{\text{one2one}} = \sum_{l=L_1}^{L_1+L_2} \mathcal{L}_{\text{Hungarian}}(\bar{\mathbf{P}}^l, \mathbf{G}). \quad (6)$$

In summary, we apply the combination of both $\mathcal{L}_{\text{one2many}}$ and $\mathcal{L}_{\text{one2one}}$ through the whole training procedure. The right of Figure 2 presents the overall pipeline.

3.3. Analysis Experiments

We choose Deformable-DETR as the baseline and compare the results based on the above three different hybrid matching approaches. To ensure fairness, we choose the settings of each hybrid matching approach as follows:

- *Baseline settings*: We use 300 or 1800 queries and apply the conventional one-to-one matching following the original Deformable-DETR [81].

- *Hybrid branch settings*: We use 300 queries for one-to-one matching branch and 1500 queries for one-to-many matching branch, i.e., $n=300$ and $T=1500$. We set K as 6 for the augmented ground truth $\hat{\mathbf{G}}$. In other words, we will generate $6\times$ additional positive queries with the one-to-many

Table 3: Object detection results on LVIS v1.0 val.

Model	Backbone	#epochs	AP
NAS-FPN + CopyPase [15]	EfficientNet-B7	48	41.6
Mask R-CNN + ViT-Det + MAE [25]	ViT-B	100	40.0
Mask R-CNN + ViT-Det + MAE [25]	ViT-L	100	46.1
Mask R-CNN + ViT-Det + MAE [25]	ViT-H	100	49.1
Deformable-DETR	R50	24	30.9
\mathcal{H} -Deformable-DETR	R50	24	33.5
Deformable-DETR	Swin-B	48	42.7
\mathcal{H} -Deformable-DETR	Swin-B	48	46.0
Deformable-DETR	Swin-L	48	43.7
\mathcal{H} -Deformable-DETR	Swin-L	48	47.5

matching branch, e.g., we have $(1+6)\times 12\times 6$ under 12× training epochs if the benchmark is the number of positive queries within one training epoch for each decoder layer.

- *Hybrid epoch settings*: We use 1800 queries through the whole training process, i.e., $M=1800$. To generate $6\times$ additional positive queries than the baseline, we set $\bar{K}=10$ and $\rho=\frac{2}{3}$. Therefore, we have $10\times\frac{2}{3}\times 12\times 6 + \frac{1}{3}\times 12\times 6 = (1+6)\times 12\times 6$ holds under 12× training epochs.

- *Hybrid layer settings*: We also use 1800 queries through the whole training process, i.e., $N=1800$. To generate $6\times$ additional positive queries than the baseline, we set $\bar{K}=10$, $L_1=4$, and $L_2=2$ considering that $10\times 12\times 4 + 12\times 2 = (1+6)\times 12\times 6$ holds.

We summarize the detailed comparison results in Table 2. Accordingly, we can see that hybrid matching approaches consistently outperform the baseline under different training epochs. We can see that the hybrid branch scheme is the best choice if we consider the trade-off of training time, inference GFLOPs/FPS, and accuracy. Therefore, we choose the hybrid branch scheme by default if not specified in the following experiments.

4. Experiment

4.1. 2D Object Detection Results

We first report the object detection results on LVIS in Table 3. Notably, the very recent ViT-Det [25] models

Table 4: Comparison results with previous DETR variants on COCO 2017 val.

Model	Backbone	MS	TS	#query	#epochs	AP	AP ₅₀	AP ₇₅	AP _S	AP _M	AP _L
Conditional-DETR [44]	R50	\times	\times	300	108	43.0	64.0	45.7	22.7	46.7	61.5
Conditional-DETR [44]	R101	\times	\times	300	108	44.5	65.6	47.5	23.6	48.4	63.6
SAM-DETR [73]	R50	\times	\times	300	50	39.8	61.8	41.6	20.5	43.4	59.6
SAM-DETR + SMCA [73]	R50	\times	\times	300	50	41.8	63.2	43.9	22.1	45.9	60.9
Anchor-DETR [62]	R50	\times	\times	300	50	42.1	63.1	44.9	22.3	46.2	60.0
Anchor-DETR [62]	R101	\times	\times	300	50	43.5	64.3	46.6	23.2	47.7	61.4
Dynamic-DETR [10]	R50	\times	\times	300	12	42.9	61.0	46.3	24.6	44.9	54.4
SMCA-DETR [13]	R50	\checkmark	\times	300	108	45.6	65.5	49.1	25.9	49.3	62.6
SMCA-DETR [13]	R101	\checkmark	\times	300	108	46.3	66.6	50.2	27.2	50.5	63.2
AdaMixer [14]	R50	\checkmark	\times	300	36	47.0	66.0	51.1	30.1	50.2	61.8
AdaMixer [14]	R101	\checkmark	\times	300	36	48.0	67.0	52.4	30.0	51.2	63.7
AdaMixer [14]	Swin-S	\checkmark	\times	300	36	51.3	71.2	55.7	34.2	54.6	67.3
CF-DETR [4]	R50	\checkmark	\times	300	36	47.8	66.5	52.4	31.2	50.6	62.8
CF-DETR [4]	R101	\checkmark	\times	300	36	49.0	68.1	53.4	31.4	52.2	64.3
Deformable-DETR [81]	R50	\checkmark	\times	300	50	46.2	65.0	50.0	28.3	49.2	61.5
Deformable-DETR [81]	R50	\checkmark	\checkmark	300	50	46.9	65.6	51.0	29.6	50.1	61.6
Sparse-DETR [52]	R50	\checkmark	\checkmark	300	50	46.3	66.0	50.1	29.0	49.5	60.8
Sparse-DETR [52]	Swin-T	\checkmark	\checkmark	300	50	49.3	69.5	53.3	32.0	52.7	64.9
Efficient-DETR [68]	R50	\checkmark	\checkmark	300	36	45.1	63.1	49.1	28.3	48.4	59.0
Efficient-DETR [68]	R101	\checkmark	\checkmark	300	36	45.7	64.1	49.5	28.2	49.1	60.2
DAB-Deformable-DETR [34]	R50	\checkmark	\checkmark	300	50	46.8	66.0	50.4	29.1	49.8	62.3
DN-Deformable-DETR [22]	R50	\checkmark	\checkmark	300	12	43.4	61.9	47.2	24.8	46.8	59.4
DN-Deformable-DETR [22]	R50	\checkmark	\checkmark	300	50	48.6	67.4	52.7	31.0	52.0	63.7
DN-Deformable-DETR [22]	R101	\checkmark	\checkmark	300	50	45.2	65.5	48.3	24.1	49.1	65.1
DINO-Deformable-DETR [74] [†]	R50	\checkmark	\checkmark	900	12	47.9	65.3	52.1	31.2	50.9	61.9
DINO-Deformable-DETR [74] [†]	R50	\checkmark	\checkmark	900	24	49.9	67.4	54.5	31.8	53.3	64.3
DINO-Deformable-DETR [74] [†]	R50	\checkmark	\checkmark	900	36	50.5	68.3	55.1	32.7	53.9	64.9
\mathcal{H} -Deformable-DETR	R50	\checkmark	\checkmark	300	12	48.7	66.4	52.9	31.2	51.5	63.5
\mathcal{H} -Deformable-DETR	R101	\checkmark	\checkmark	300	12	49.4	67.2	53.7	31.9	53.1	64.2
\mathcal{H} -Deformable-DETR	Swin-T	\checkmark	\checkmark	300	12	50.6	68.9	55.1	33.4	53.7	65.9
\mathcal{H} -Deformable-DETR	Swin-S	\checkmark	\checkmark	300	12	52.5	71.2	57.5	35.2	56.1	68.0
\mathcal{H} -Deformable-DETR	Swin-S (IN-22K)	\checkmark	\checkmark	300	12	53.5	72.3	58.4	36.6	57.1	69.4
\mathcal{H} -Deformable-DETR	Swin-L (IN-22K)	\checkmark	\checkmark	300	12	55.9	75.2	61.0	39.1	59.9	72.2
\mathcal{H} -Deformable-DETR	Swin-L (IN-22K)	\checkmark	\checkmark	900	12	56.1	75.2	61.3	39.3	60.4	72.4
\mathcal{H} -Deformable-DETR	R50	\checkmark	\checkmark	300	36	50.0	68.3	54.4	32.9	52.7	65.3
\mathcal{H} -Deformable-DETR	R101	\checkmark	\checkmark	300	36	50.1	68.4	54.5	31.7	53.6	65.3
\mathcal{H} -Deformable-DETR	Swin-T	\checkmark	\checkmark	300	36	53.2	71.5	58.2	35.9	56.4	68.2
\mathcal{H} -Deformable-DETR	Swin-S	\checkmark	\checkmark	300	36	54.4	72.9	59.4	36.9	58.3	69.5
\mathcal{H} -Deformable-DETR	Swin-S (IN-22K)	\checkmark	\checkmark	300	36	55.3	74.4	60.5	38.3	58.9	72.0
\mathcal{H} -Deformable-DETR	Swin-L (IN-22K)	\checkmark	\checkmark	300	36	57.1	76.2	62.5	39.7	61.4	73.4
\mathcal{H} -Deformable-DETR	Swin-L (IN-22K)	\checkmark	\checkmark	900	36	57.4	76.2	63.0	41.1	61.5	73.9
\mathcal{H} -Deformable-DETR [†]	Swin-L (IN-22K)	\checkmark	\checkmark	900	36	57.6	76.5	63.2	41.4	61.7	73.9

MS: multi-scale features. TS: two-stage. [†]: keep 300 instead of 100 predictions for evaluation. #query: the number of queries used during evaluation.

are trained with both bounding boxes and instance masks supervision while we only apply bounding boxes supervision. Our approach achieves significant gains over the baseline Deformable-DETR, e.g., with Swin-L as the backbone, \mathcal{H} -Deformable-DETR improves the AP score by +3.8%, where part of the improvement comes from other tricks and we provide more details in the ablation experiments and supplementary.

Table 4 reports the comparisons on COCO object detection val set. We can see that our \mathcal{H} -Deformable-DETR achieves comparable performance with the very recent DINO-Deformable-DETR [74]. For example, when using

12× training epochs with ResNet-50, our \mathcal{H} -Deformable-DETR achieves 48.7% while DINO-Deformable-DETR achieves 47.9% by applying a more complex contrastive denoising training scheme based on the redesigned query formulation, i.e., (cx, cy, h, w) , of DAB-DETR [34].

According to Table 4, with ResNet-50 as the backbone, DINO-Deformable-DETR achieves better performance under 36× training epochs, which is related to two modifications, including keeping more predictions for evaluation and increasing the number of queries during evaluation. We also show that applying these two modifications further improves the performance of our \mathcal{H} -Deformable-DETR with

Swin-L from 57.1% to 57.6% under single-scale testing.

4.2. 3D Object Detection Results

We choose two representative DETR-based approaches, including 3DETR [46] and the very recent PETRv2 [37], to verify the generalization ability of our approach for 3D detection based on either point clouds or multi-view images. Table 5 and Table 6 summarize the detailed comparison results. We can see that our \mathcal{H} -PETRv2 significantly improves the NDS scores of baseline PETRv2 from 50.68% to 52.38% on nuScenes val. Besides, our \mathcal{H} -3DETR-m also achieves significant gains on AP₅₀ metrics on ScanNetV2 val, thus showing that our hybrid matching improves the localization accuracy of 3D object detection predictions.

4.3. Multi-Person Pose Estimation Results

We extend our hybrid matching strategy to the very recent PETR (Pose Estimation with TRansformers) [53] and summarize the detailed results in Table 7. We can see that our approach achieves consistent gains over the baselines. For example, with Swin-L as the backbone, our \mathcal{H} -PETR improves the AP score of PETR from 73.3% to 74.9% on the COCO val.

4.4. Multi-Object Tracking Results

Last, we further apply our hybrid matching scheme to a very powerful multi-object tracking approach, e.g., TransTrack [55]. Table 8 summarizes the detailed comparison results. We find the results on MOT17 suffer from relatively large variance, thus we report the mean performance with ~ 3 runs. Accordingly, our approach also shows strong potential on the multi-object tracking tasks, and our \mathcal{H} -TransTrack improves the MOTA score of TransTrack from 67.1% to 68.7% on MOT17 val, where we also observe that the gains are related to much lower false negative rates.

4.5. Ablation study

The effect of each component based on Deformable-DETR. We report the detailed improvements of each component in Table 9. Notably, we do not observe the obvious benefits of applying drop-out rate as zero, mixed query selection, and looking forward twice¹ in other tasks. Therefore, we only apply this combination of tricks on 2D object detection tasks by default if not specified. We further analyze the detailed improvements of our approach based on the metrics of optimal localization recall precision in Figure 5, where the lower the better. In summary, we can see that our approach mainly improves the performance from

¹We implement both mixed query selection and looking forward twice following DINO [74].

two aspects, including more accurate localization and fewer false negatives.

Influence of the loss weights on the one-to-many matching branch. We study the influence of the loss weight λ associated with the one-to-many matching loss $\mathcal{L}_{\text{one2many}}$ in Table 10. We can see that our approach is not sensitive to the choice of λ and we simply choose $\lambda=1$ for all experiments by default.

The choice of K within the one-to-many matching branch. We study the influence of the choice of K in Table 11. Accordingly, we find our approach achieves consistent gains only when choosing K larger than 3. We choose K as 6 on COCO by default. We guess the reasons for the performance drop when setting smaller values are related to the lower quality of the queries due to the two-stage mechanism [81], which ranks the queries according to their classification confidence score. We also show that designing a careful selection mechanism for the one-to-many matching branch can achieve consistent gains even when using $K=1$ but do not observe any further benefits when using large K values. More details are summarized in the supplementary.

The number of queries T within the one-to-many matching branch. We study the influence of the total number of queries T within the one-to-many matching branch by fixing K as 6 in Table 12. We choose $T=1500$ on the COCO object detection task as it achieves the best results.

Influence of sharing parameters. We study the influence of the sharing parameters across the one-to-one matching branch and one-to-many matching branch in Table 13. We can observe that (i) using independent classification heads or bounding box heads does not hurt the performance, (ii) further using independent transformer decoder layers slightly drops, and (iii) further using independent transformer encoder layers results in significant performance drops considering the baseline performance is 47.0%.

Comparison to only using one-to-many matching. Table 14 compares our approach to a strong variant that applies only one-to-many matching through the whole training process and NMS during evaluation. We also ablate the predictions based only on the one-to-one matching branch or one-to-many matching branch in Table 14. Accordingly, we see that (i) the one-to-many branch evaluated with NMS achieves comparable performance with the one-to-one matching branch; (ii) only using one-to-many matching evaluated with NMS achieves slightly better performance than ours; (ii) the one-to-one matching branch within our hybrid matching scheme is the best choice when considering the training time and inference speed (FPS).

Comparison to longer training epochs. We investigate whether training Deformable-DETR for longer helps in Figure 6. We further analyze the training losses and validation losses in Figure 3. Accordingly, we can see that sim-

Table 5: Multi-view 3D detection results on nuScenes.

Method	Backbone	#epochs	mAP	NDS
PETRv2 [37]	VoVNet-99	24	41.04	50.25
PETRv2 (Our repro.)	VoVNet-99	24	40.41	49.69
PETRv2 (Our repro.)	VoVNet-99	36	41.07	50.68
\mathcal{H} -PETRv2	VoVNet-99	24	41.93	51.23
\mathcal{H} -PETRv2	VoVNet-99	36	<u>42.59</u>	<u>52.38</u>

Table 7: Multi-person pose estimation results on COCO.

Method	Backbone	#epochs	AP	AP ₅₀	AP ₇₅	AP _M	AP _L
PETR [53]	R50	100	68.8	87.5	76.3	62.7	77.7
PETR (Our repro.)	R50	100	69.3	88.2	76.8	63.3	78.4
\mathcal{H} -PETR	R50	100	<u>70.9</u>	<u>89.0</u>	<u>78.2</u>	<u>64.4</u>	<u>80.3</u>
PETR [53]	R101	100	70.0	88.5	77.5	63.6	79.4
PETR (Our repro.)	R101	100	69.9	88.3	76.8	63.4	79.4
\mathcal{H} -PETR	R101	100	<u>71.0</u>	<u>89.6</u>	<u>78.2</u>	<u>64.7</u>	<u>80.2</u>
PETR [53]	Swin-L	100	73.1	90.7	80.9	67.2	81.7
PETR (Our repro.)	Swin-L	100	73.3	90.6	80.8	67.7	81.6
\mathcal{H} -PETR	Swin-L	100	<u>74.9</u>	<u>91.3</u>	<u>82.3</u>	<u>69.3</u>	<u>83.3</u>

Table 9: Comparison results based on two-stage Deformable-DETR on COCO 2017 `val` under 12× epochs schedule. 2×FFN: increase FFN dimension from 1,024 to 2,048. DPO: setting the drop out rate within transformer as 0. MQS: mixed query selection. LFT: look forward twice. HM: our hybrid matching.

2×FFN	DPO	MQS	LFT	HM	AP
✗	✗	✗	✗	✗	43.3
✓	✗	✗	✗	✗	43.7
✓	✓	✗	✗	✗	44.3
✓	✓	✓	✗	✗	46.3
✓	✓	✓	✓	✗	47.0
✓	✓	✓	✓	✓	<u>48.7</u>

Table 10: Influence of λ of our approach on COCO 2017 `val` under 12× epochs training schedule. We set $K = 6$ and $T = 1500$.

λ	0.1	0.2	0.5	1	2	5
AP	47.8	48.0	48.4	<u>48.7</u>	48.5	48.3

Table 11: Influence of K of our approach on COCO 2017 `val` under 12× epochs schedule. We set $T = 300 \times K$.

K	0	1	2	3	4	5	6	7	8
AP	47.0	46.4	46.7	48.1	48.4	48.3	<u>48.6</u>	48.5	<u>48.6</u>

ply increasing the number of training epochs fails to improve the performance. In other words, Deformable-DETR can not benefit from exploring more positive queries that are matched with ground truth during the additional training epochs, which also verifies the advantage of our hybrid matching scheme.

Analyzing the loss curves of the one-to-one matching

Table 6: 3D detection results on ScanNetV2.

Method	#epochs	AP ₂₅	AP ₅₀
3DETR-m [46]	180	58.70	33.60
3DETR-m (Our repro.)	180	57.17	29.34
\mathcal{H} -3DETR-m	180	<u>59.86</u>	<u>34.01</u>
3DETR-m [46]	720	63.70	44.50
3DETR-m (Our repro.)	720	64.50	45.45
\mathcal{H} -3DETR-m	720	<u>64.74</u>	<u>47.01</u>

Table 7: Multi-object tracking results on MOT.

Model	#epochs	MOTA	IDF1	FN
MOT17 val				
TransTrack [55]	20	67.1	70.3	15820
TransTrack (Our repro.)	20	67.1	68.1	15680
\mathcal{H} -TransTrack	20	<u>68.7</u>	<u>68.3</u>	<u>13657</u>
MOT17 test				
TransTrack [55]	20	74.5	63.9	112137
TransTrack (Our repro.)	20	74.6	63.2	111105
\mathcal{H} -TransTrack	20	<u>75.7</u>	<u>64.4</u>	<u>91155</u>

Table 12: Influence of T of our approach on COCO 2017 `val` under 12× epochs schedule. We set $K = 6$.

T	300	600	900	1200	1500	1800
AP	47.8	48.3	48.4	48.4	<u>48.7</u>	48.6

Table 13: Influence of sharing parameters.

trans. encoder	trans. decoder	box head	cls head	AP
✓	✓	✓	✓	<u>48.7</u>
✓	✓	✓	✗	48.6
✓	✓	✗	✗	48.5
✓	✗	✗	✗	48.3
✗	✗	✗	✗	47.3

Table 14: Comparison to only using one-to-many matching.

Method	NMS	Time (average)	FPS	#epochs		
				12	24	36
Only one-to-many matching	✓	95min	5.3	49.4	<u>50.2</u>	48.8
Ours (one-to-one branch)	✗		6.7	48.7	49.9	50.0
Ours (one-to-one branch)	✓	85min	5.6	48.7	50.0	50.0
Ours (one-to-many branch)	✗		6.5	13.5	13.1	12.9
Ours (one-to-many branch)	✓		5.4	48.6	49.8	49.9

branch. We illustrate the loss curves of our \mathcal{H} -Deformable-DETR and the baseline Deformable-DETR in Figure 4. To ensure fairness, we only consider the $\mathcal{L}_{\text{one2one}}$ through the whole training procedure. Accordingly, we can see our approach achieves both lower training loss values and lower validation loss values, which shows that the additional one-to-many matching branch could ease the optimization of the one-to-one matching branch.

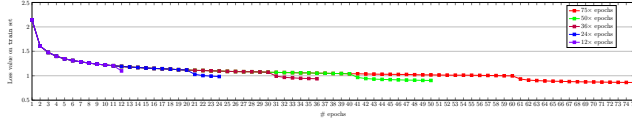


Figure 3: Illustrating the loss curves of Deformable-DETR on train and val. We can see that, with longer training epochs, e.g., from 50 epochs to 75 epochs, the training loss consistently decreases while the validation loss saturates on COCO object detection benchmark.

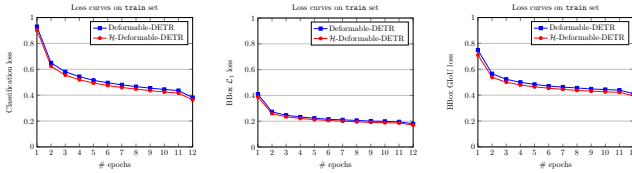
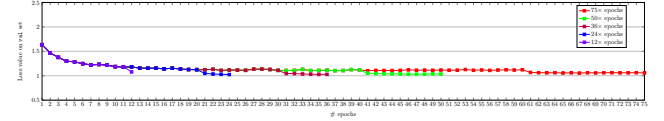


Figure 4: Illustrating the loss curves on train and val. Our approach helps the optimization of Deformable-DETR, thus decreasing the loss values on both train and val of COCO object detection benchmark.

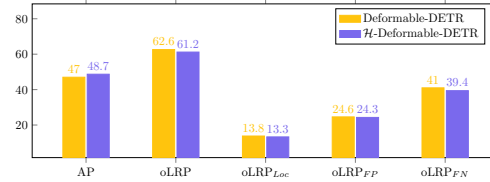


Figure 5: Illustrating the improvements of hybrid matching over Deformable-DETR. We report both average precision (AP) and optimal localization recall precision (oLRP [48]) scores, where the higher the better for AP and the lower the better for oLRP. Our approach significantly decreases oLRP_{Loc} and oLRP_{FN}, which represent the localization error of matched detections (true positives) and the number of unmatched ground truth (false negatives).

5. Conclusion

This paper presents a very simple yet surprisingly effective hybrid matching scheme to address the low training efficiency of DETR-based approaches on multiple vision tasks. Our approach explicitly combines the advantages of a one-to-one matching scheme, i.e., avoiding NMS, and those of a one-to-many matching scheme, i.e., increasing the number of positive queries and training efficiency. We hope our initial efforts can accelerate the advancement of DETR approaches on various vision tasks.

6. Acknowledgement

We thank Di He, Zheng Zhang, Jin-Ge Yao, Yue Cao, and Yili Wang for helpful discussions. Especially, Yili Wang helps to verify the proposed method for multi-person pose estimation tasks at the early stage.

References

- [1] X. Bai, Z. Hu, X. Zhu, Q. Huang, Y. Chen, H. Fu, and C.-L. Tai. Transfusion: Robust lidar-camera fusion for 3d object detection with transformers. In *CVPR*, pages 1090–1099, 2022. [1](#), [2](#)
- [2] G. Brasó, N. Kister, and L. Leal-Taixé. The center of attention: Center-keypoint grouping via attention for multi-person pose estimation. In *ICCV*, pages 11853–11863, 2021. [2](#)
- [3] H. Caesar, V. Bankiti, A. H. Lang, S. Vora, V. E. Liong, Q. Xu, A. Krishnan, Y. Pan, G. Baldan, and O. Beijbom. nuscenes: A multimodal dataset for autonomous driving. In *CVPR*, pages 11621–11631, 2020. [12](#)
- [4] X. Cao, P. Yuan, B. Feng, K. Niu, and Y. Zhao. Cf-detr: Coarse-to-fine transformers for end-to-end object detection. In *AAAI*, 2022. [1](#), [3](#), [6](#)
- [5] N. Carion, F. Massa, G. Synnaeve, N. Usunier, A. Kirillov, and S. Zagoruyko. End-to-end object detection with transformers. In *European conference on computer vision*, pages 213–229. Springer, 2020. [1](#), [2](#), [3](#), [4](#)
- [6] X. Chen, B. Yan, J. Zhu, D. Wang, X. Yang, and H. Lu. Transformer tracking. In *CVPR*, pages 8126–8135, 2021. [1](#)
- [7] B. Cheng, A. Choudhuri, I. Misra, A. Kirillov, R. Girdhar, and A. G. Schwing. Mask2former for video instance segmentation. *arXiv preprint arXiv:2112.10764*, 2021. [1](#)
- [8] B. Cheng, I. Misra, A. G. Schwing, A. Kirillov, and R. Girdhar. Masked-attention mask transformer for universal image segmentation. *arXiv preprint arXiv:2112.01527*, 2021. [1](#), [3](#)
- [9] A. Dai, A. X. Chang, M. Savva, M. Halber, T. Funkhouser, and M. Nießner. Scannet: Richly-annotated 3d reconstruc-

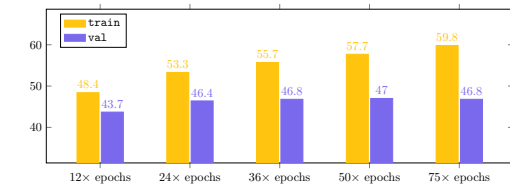


Figure 6: Illustrating the AP scores of Deformable-DETR on train and val under longer training epochs. We can see that, with longer training epochs, e.g., from 50 epochs to 75 epochs, the AP scores on train set consistently improves while the AP scores on val set saturates on COCO object detection benchmark.

tions of indoor scenes. In *CVPR*, pages 5828–5839, 2017. 12

[10] X. Dai, Y. Chen, J. Yang, P. Zhang, L. Yuan, and L. Zhang. Dynamic detr: End-to-end object detection with dynamic attention. In *Proceedings of the IEEE/CVF International Conference on Computer Vision*, pages 2988–2997, 2021. 2, 6

[11] B. Dong, F. Zeng, T. Wang, X. Zhang, and Y. Wei. Solq: Segmenting objects by learning queries. *NeurIPS*, 2021. 1

[12] Y. Fang, S. Yang, X. Wang, Y. Li, C. Fang, Y. Shan, B. Feng, and W. Liu. Instances as queries. In *ICCV*, pages 6910–6919, October 2021. 1

[13] P. Gao, M. Zheng, X. Wang, J. Dai, and H. Li. Fast convergence of detr with spatially modulated co-attention. In *ICCV*, pages 3621–3630, 2021. 1, 2, 6

[14] Z. Gao, L. Wang, B. Han, and S. Guo. Adamixer: A fast-converging query-based object detector. In *CVPR*, 2022. 1, 6

[15] G. Ghiasi, Y. Cui, A. Srinivas, R. Qian, T.-Y. Lin, E. D. Cubuk, Q. V. Le, and B. Zoph. Simple copy-paste is a strong data augmentation method for instance segmentation. In *CVPR*, pages 2918–2928, 2021. 5

[16] R. Girshick. Fast r-cnn. In *ICCV*, pages 1440–1448, 2015. 2

[17] B. A. Griffin and J. J. Corso. Depth from camera motion and object detection. In *CVPR*, pages 1397–1406, 2021. 1

[18] A. Gupta, P. Dollar, and R. Girshick. Lvis: A dataset for large vocabulary instance segmentation. In *CVPR*, pages 5356–5364, 2019. 12

[19] J. Huang and G. Huang. Bevdet4d: Exploit temporal cues in multi-camera 3d object detection. *arXiv preprint arXiv:2203.17054*, 2022. 2

[20] J. Huang, G. Huang, Z. Zhu, and D. Du. Bevdet: High-performance multi-camera 3d object detection in bird-eye-view. *arXiv preprint arXiv:2112.11790*, 2021. 2

[21] A. Kamath, M. Singh, Y. LeCun, G. Synnaeve, I. Misra, and N. Carion. Mdetr-modulated detection for end-to-end multi-modal understanding. In *ICCV*, pages 1780–1790, 2021. 1

[22] F. Li, H. Zhang, S. Liu, J. Guo, L. M. Ni, and L. Zhang. Dn-detr: Accelerate detr training by introducing query denoising. *arXiv preprint arXiv:2203.01305*, 2022. 1, 2, 3, 6

[23] F. Li, H. Zhang, S. Liu, L. Zhang, L. M. Ni, H.-Y. Shum, et al. Mask dino: Towards a unified transformer-based framework for object detection and segmentation. *arXiv preprint arXiv:2206.02777*, 2022. 1

[24] K. Li, S. Wang, X. Zhang, Y. Xu, W. Xu, and Z. Tu. Pose recognition with cascade transformers. In *CVPR*, pages 1944–1953, 2021. 1, 2

[25] Y. Li, H. Mao, R. Girshick, and K. He. Exploring plain vision transformer backbones for object detection. *arXiv preprint arXiv:2203.16527*, 2022. 5

[26] Y. Li, S. Zhang, Z. Wang, S. Yang, W. Yang, S.-T. Xia, and E. Zhou. Tokenpose: Learning keypoint tokens for human pose estimation. In *ICCV*, pages 11313–11322, 2021. 2

[27] Z. Li, Z. Chen, X. Liu, and J. Jiang. Depthformer: Exploiting long-range correlation and local information for accurate monocular depth estimation. *arXiv preprint arXiv:2203.14211*, 2022. 1

[28] Z. Li, W. Wang, H. Li, E. Xie, C. Sima, T. Lu, Q. Yu, and J. Dai. Bevformer: Learning bird’s-eye-view representation from multi-camera images via spatiotemporal transformers. *arXiv preprint arXiv:2203.17270*, 2022. 1, 2

[29] Z. Li, W. Wang, E. Xie, Z. Yu, A. Anandkumar, J. M. Alvarez, P. Luo, and T. Lu. Panoptic segformer: Delving deeper into panoptic segmentation with transformers. In *CVPR*, pages 1280–1289, 2022. 1, 3

[30] Z. Li, X. Wang, X. Liu, and J. Jiang. Binsformer: Revisiting adaptive bins for monocular depth estimation. *arXiv preprint arXiv:2204.00987*, 2022. 3

[31] T. Liang, H. Xie, K. Yu, Z. Xia, Z. Lin, Y. Wang, T. Tang, B. Wang, and Z. Tang. Bevfusion: A simple and robust lidar-camera fusion framework. *arXiv preprint arXiv:2205.13790*, 2022. 2

[32] T.-Y. Lin, P. Goyal, R. Girshick, K. He, and P. Dollár. Focal loss for dense object detection. In *Proceedings of the IEEE international conference on computer vision*, pages 2980–2988, 2017. 2, 3

[33] T.-Y. Lin, M. Maire, S. Belongie, J. Hays, P. Perona, D. Ramanan, P. Dollár, and C. L. Zitnick. Microsoft coco: Common objects in context. In *ECCV*, pages 740–755. Springer, 2014. 12

[34] S. Liu, F. Li, H. Zhang, X. Yang, X. Qi, H. Su, J. Zhu, and L. Zhang. Dab-detr: Dynamic anchor boxes are better queries for detr. *arXiv preprint arXiv:2201.12329*, 2022. 1, 2, 3, 6

[35] W. Liu, D. Anguelov, D. Erhan, C. Szegedy, S. Reed, C.-Y. Fu, and A. C. Berg. Ssd: Single shot multibox detector. In *ECCV*, pages 21–37. Springer, 2016. 2

[36] Y. Liu, T. Wang, X. Zhang, and J. Sun. Petr: Position embedding transformation for multi-view 3d object detection. *arXiv preprint arXiv:2203.05625*, 2022. 2

[37] Y. Liu, J. Yan, F. Jia, S. Li, Q. Gao, T. Wang, X. Zhang, and J. Sun. PetrV2: A unified framework for 3d perception from multi-camera images. *arXiv preprint arXiv:2206.01256*, 2022. 2, 7, 8

[38] Z. Liu, H. Tang, A. Amini, X. Yang, H. Mao, D. Rus, and S. Han. Bevfusion: Multi-task multi-sensor fusion with unified bird’s-eye view representation. *arXiv preprint arXiv:2205.13542*, 2022. 2

[39] Z. Liu, Z. Zhang, Y. Cao, H. Hu, and X. Tong. Group-free 3d object detection via transformers. In *ICCV*, pages 2949–2958, 2021. 2

[40] S. Long, S. Qin, D. Panteleev, A. Bissacco, Y. Fujii, and M. Raptis. Towards end-to-end unified scene text detection and layout analysis. In *CVPR*, pages 1049–1059, 2022. 1

[41] Q. Lou, Y.-C. Hsu, B. Uzkent, T. Hua, Y. Shen, and H. Jin. Lite-mdetr: A lightweight multi-modal detector. In *CVPR*, pages 12206–12215, 2022. 1

[42] W. Mao, Y. Ge, C. Shen, Z. Tian, X. Wang, and Z. Wang. Tfpose: Direct human pose estimation with transformers. *arXiv preprint arXiv:2103.15320*, 2021. 2

[43] T. Meinhardt, A. Kirillov, L. Leal-Taixe, and C. Feichtenhofer. Trackformer: Multi-object tracking with transformers. In *CVPR*, pages 8844–8854, 2022. 1, 3

[44] D. Meng, X. Chen, Z. Fan, G. Zeng, H. Li, Y. Yuan, L. Sun, and J. Wang. Conditional detr for fast training convergence. In *Proceedings of the IEEE International Conference on Computer Vision (ICCV)*, 2021. [1](#), [2](#), [3](#), [6](#)

[45] A. Milan, L. Leal-Taixé, I. Reid, S. Roth, and K. Schindler. Mot16: A benchmark for multi-object tracking. *arXiv preprint arXiv:1603.00831*, 2016. [12](#)

[46] I. Misra, R. Girdhar, and A. Joulin. An end-to-end transformer model for 3d object detection. In *ICCV*, pages 2906–2917, 2021. [1](#), [2](#), [7](#), [8](#)

[47] A. Neubeck and L. Van Gool. Efficient non-maximum suppression. In *ICPR*, volume 3, pages 850–855, 2006. [2](#)

[48] K. Oksuz, B. C. Cam, S. Kalkan, and E. Akbas. One metric to measure them all: Localisation recall precision (lrp) for evaluating visual detection tasks. *PAMI*, 2021. [9](#)

[49] Z. Raisi, M. A. Naei, G. Younes, S. Wardell, and J. S. Zelek. Transformer-based text detection in the wild. In *CVPR*, pages 3162–3171, 2021. [1](#)

[50] Z. Raisi, G. Younes, and J. Zelek. Arbitrary shape text detection using transformers. *arXiv preprint arXiv:2202.11221*, 2022. [1](#)

[51] S. Ren, K. He, R. Girshick, and J. Sun. Faster r-cnn: Towards real-time object detection with region proposal networks. *Advances in neural information processing systems*, 28, 2015. [2](#), [3](#)

[52] B. Roh, J. Shin, W. Shin, and S. Kim. Sparse detr: Efficient end-to-end object detection with learnable sparsity. *arXiv preprint arXiv:2111.14330*, 2021. [1](#), [6](#)

[53] D. Shi, X. Wei, L. Li, Y. Ren, and W. Tan. End-to-end multi-person pose estimation with transformers. In *Proceedings of the IEEE/CVF Conference on Computer Vision and Pattern Recognition*, pages 11069–11078, 2022. [1](#), [2](#), [3](#), [7](#), [8](#)

[54] L. Stoffl, M. Vidal, and A. Mathis. End-to-end trainable multi-instance pose estimation with transformers. *arXiv preprint arXiv:2103.12115*, 2021. [1](#), [2](#)

[55] P. Sun, J. Cao, Y. Jiang, R. Zhang, E. Xie, Z. Yuan, C. Wang, and P. Luo. Trantrack: Multiple object tracking with transformer. *arXiv preprint arXiv:2012.15460*, 2020. [1](#), [2](#), [3](#), [7](#), [8](#), [12](#)

[56] Z. Tian, C. Shen, H. Chen, and T. He. Fcos: Fully convolutional one-stage object detection. In *Proceedings of the IEEE/CVF international conference on computer vision*, pages 9627–9636, 2019. [3](#)

[57] A. Vaswani, N. Shazeer, N. Parmar, J. Uszkoreit, L. Jones, A. N. Gomez, L. u. Kaiser, and I. Polosukhin. Attention is all you need. In *NeurIPS*, 2017. [2](#)

[58] H. Wang, Y. Zhu, H. Adam, A. Yuille, and L.-C. Chen. Max-deeplab: End-to-end panoptic segmentation with mask transformers. In *CVPR*, pages 5463–5474, 2021. [1](#)

[59] J. Wang, L. Song, Z. Li, H. Sun, J. Sun, and N. Zheng. End-to-end object detection with fully convolutional network. In *CVPR*, pages 15849–15858, 2021. [1](#), [3](#)

[60] W. Wang, J. Zhang, Y. Cao, Y. Shen, and D. Tao. Towards data-efficient detection transformers. *arXiv preprint arXiv:2203.09507*, 2022. [2](#)

[61] Y. Wang, V. C. Guizilini, T. Zhang, Y. Wang, H. Zhao, and J. Solomon. Detr3d: 3d object detection from multi-view images via 3d-to-2d queries. In *Conference on Robot Learning*, pages 180–191. PMLR, 2022. [1](#), [2](#)

[62] Y. Wang, X. Zhang, T. Yang, and J. Sun. Anchor detr: Query design for transformer-based detector, 2021. [1](#), [2](#), [3](#), [6](#)

[63] J. Wu, Y. Jiang, P. Sun, Z. Yuan, and P. Luo. Language as queries for referring video object segmentation. *arXiv preprint arXiv:2201.00487*, 2022. [1](#)

[64] J. Wu, Y. Jiang, W. Zhang, X. Bai, and S. Bai. Seqformer: a frustratingly simple model for video instance segmentation. *arXiv preprint arXiv:2112.08275*, 2021. [1](#)

[65] Y. Xu, W. Xu, D. Cheung, and Z. Tu. Line segment detection using transformers without edges. In *CVPR*, pages 4257–4266, 2021. [1](#)

[66] B. Yan, H. Peng, J. Fu, D. Wang, and H. Lu. Learning spatio-temporal transformer for visual tracking. In *ICCV*, pages 10448–10457, 2021. [3](#)

[67] Z. Yang, J. Wang, Y. Tang, K. Chen, H. Zhao, and P. H. Torr. Lavt: Language-aware vision transformer for referring image segmentation. In *CVPR*, pages 18155–18165, 2022. [1](#)

[68] Z. Yao, J. Ai, B. Li, and C. Zhang. Efficient detr: improving end-to-end object detector with dense prior. *arXiv preprint arXiv:2104.01318*, 2021. [6](#)

[69] Q. Yu, H. Wang, D. Kim, S. Qiao, M. Collins, Y. Zhu, H. Adam, A. Yuille, and L.-C. Chen. Cmt-deeplab: Clustering mask transformers for panoptic segmentation. In *CVPR*, pages 2560–2570, June 2022. [1](#)

[70] X. Yu, D. Shi, X. Wei, Y. Ren, T. Ye, and W. Tan. Soit: Segmenting objects with instance-aware transformers. *arXiv preprint arXiv:2112.11037*, 2021. [1](#)

[71] Y. Yuan, X. Chen, and J. Wang. Object-contextual representations for semantic segmentation. In *European conference on computer vision*, pages 173–190. Springer, 2020. [1](#)

[72] F. Zeng, B. Dong, T. Wang, X. Zhang, and Y. Wei. Motr: End-to-end multiple-object tracking with transformer. *arXiv preprint arXiv:2105.03247*, 2021. [3](#)

[73] G. Zhang, Z. Luo, Y. Yu, K. Cui, and S. Lu. Accelerating DETR convergence via semantic-aligned matching. In *CVPR*, 2022. [1](#), [6](#)

[74] H. Zhang, F. Li, S. Liu, L. Zhang, H. Su, J. Zhu, L. M. Ni, and H.-Y. Shum. Dino: Detr with improved denoising anchor boxes for end-to-end object detection. *arXiv preprint arXiv:2203.03605*, 2022. [1](#), [2](#), [6](#), [7](#)

[75] J. Zhang, Y. Cai, S. Yan, J. Feng, et al. Direct multi-view multi-person 3d pose estimation. *NIPS*, 34:13153–13164, 2021. [2](#)

[76] S. Zhang, C. Chi, Y. Yao, Z. Lei, and S. Z. Li. Bridging the gap between anchor-based and anchor-free detection via adaptive training sample selection. In *CVPR*, 2020. [3](#)

[77] X. Zhang, Y. Su, S. Tripathi, and Z. Tu. Text spotting transformers. In *CVPR*, pages 9519–9528, 2022. [1](#)

[78] M. Zhao, K. Okada, and M. Inaba. Trtr: Visual tracking with transformer. *arXiv preprint arXiv:2105.03817*, 2021. [3](#)

[79] X. Zhou, R. Girdhar, A. Joulin, P. Krähenbühl, and I. Misra. Detecting twenty-thousand classes using image-level supervision. *arXiv preprint arXiv:2201.02605*, 2022. [12](#)

[80] B. Zhu, J. Wang, Z. Jiang, F. Zong, S. Liu, Z. Li, and J. Sun. Autoassign: Differentiable label assignment for dense object detection. *arXiv preprint arXiv:2007.03496*, 2020. [3](#)

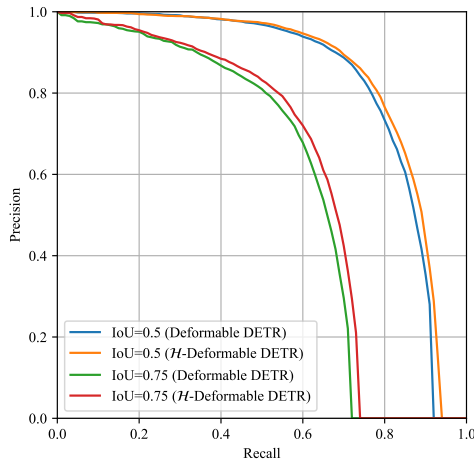


Figure 7: Illustrating the curves of Precision-Recall.

[81] X. Zhu, W. Su, L. Lu, B. Li, X. Wang, and J. Dai. Deformable detr: Deformable transformers for end-to-end object detection. *arXiv preprint arXiv:2010.04159*, 2020. 1, 2, 3, 4, 5, 6, 7

Supplementary

A. Datasets

COCO [33]. The COCO object detection dataset consists of 123K images with 896K annotated bounding boxes belonging to 80 thing classes and 53 stuff classes, where the `train` set contains 118K images and the `val` set contains 5K images. We report the 2D object detection performance on the `val` set. The COCO pose estimation benchmark consists of more than 200K images and 250K person instances labeled with 17 keypoints, where `train` set consists of 57K images and 150K person instances, `val` set consists of 5K images, and `test-dev` set consists of 20K images, respectively.

LVIS [18]. This dataset consists of 100K images annotated with both object detection bounding boxes and instance segmentation masks for 1203 classes. We follow the very recent work Detic [79] to only use the bounding box supervision for training.

nuScenes [3]. This is a large-scale autonomous driving dataset consisting of 1000 driving sequences with each one about 20s long, where the multimodel dataset is collected from 6 cameras, 1 lidar, and 5 radars. We partition the 1000 driving sequences to 700, 150, and 150 sequences for `train`, `val`, and `test` respectively. We report both the numbers of nuScenes Detection Score (NDS) and mean Average Precision (mAP) to measure the 3D object detection performance.

ScanNetV2 [9]. This dataset consists of 1513 indoor scenes labeled with per-point instance ids, semantic categories and

Table 15: Illustrating the hyper-parameter settings. $2 \times \text{FFN}$: increase FFN dimension from 1,024 to 2,048. DP0: setting the drop out rate within transformer as 0. MQS: mixed query selection. LFT: look forward twice.

Method	$2 \times \text{FFN}$	DP0	MQS	LFT	Dataset	n	T	K	λ
\mathcal{H} -Deformable-DETR	✓	✓	✓	✓	COCO	300	1500	6	1.0
					LVIS	300	900	5	1.0
\mathcal{H} -PETR	✓	✓	✗	✗	COCO	300	900	5	1.0
\mathcal{H} -PETRv2	✗	✗	✗	✗	nuScenes	900	1800	4	1.0
\mathcal{H} -3DETR-m	✗	✗	✗	✗	ScanNetV2	256	512	2	1.0
\mathcal{H} -TransTrack	✗	✗	✗	✗	MOT17	500	1000	5	0.5

3D bounding boxes for around 18 categories. We use 1201 and 312 scenes for `train` and `val`, respectively. We mainly report the mAP scores under two different IoU thresholds, i.e., 0.25 and 0.5.

MOT17 [45]. This dataset consists of 14 pedestrian tracking videos annotated with rich bounding boxes and their corresponding track ids. We use 7 videos for `train` and the other 7 videos for `test`. Following TransTrack [55], we split the second half of each `train` video to form a `val` set. We report the multi-object tracking performance on both `val` and `test`.

B. More Hyper-parameter Details

We illustrate the detailed hyper-parameter settings when applying our hybrid branch approach to different DETR-based approaches in the following Table 15.

C. Precision-Recall Curves

We compare the precision-recall curves of the baseline and our hybrid matching scheme in Figure 7. It can be seen that our approach mainly improves the recall rate of the baseline method, thus also ensuring the lower false negative rates.